Report

Cell Reports

Regulatory T Cells Restrain Pathogenic T Helper Cells during Skin Inflammation

Graphical Abstract

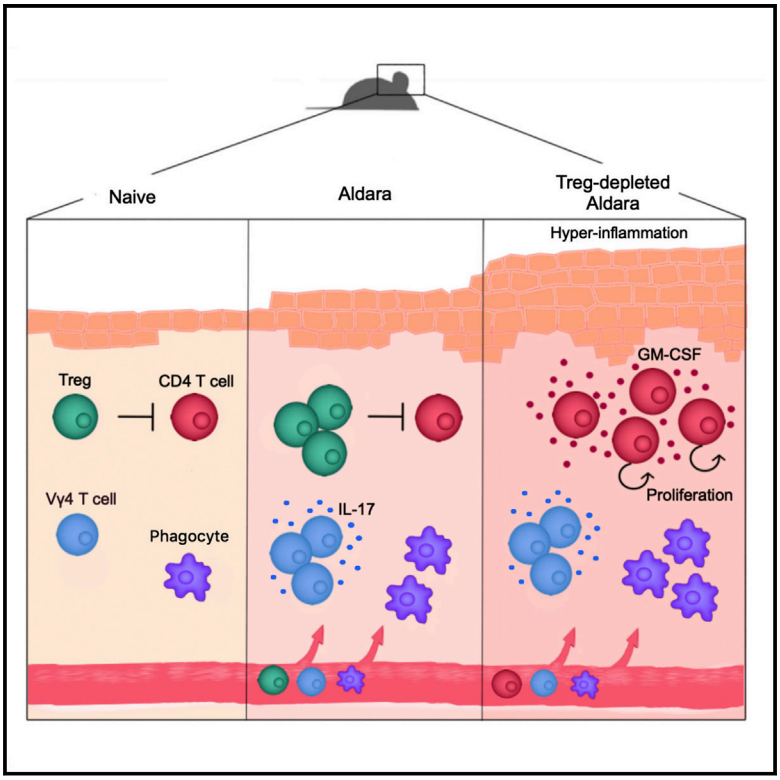

Authors

Tom Hartwig, Pascale Zwicky, Bettina Schreiner, ..., Curdin Conrad, Christoph Schlapbach, Burkhard Becher

Correspondence

becher@immunology.uzh.ch

In Brief

The contribution of Treg cells to psoriasis is poorly understood. By combining inducible depletion of Treg cells with the Aldara model of psoriasiform inflammation, Hartwig et al. reveal a non-redundant role of Treg cells in promoting the remission of skin inflammation by limiting invasion of $CD4^+$ GM-CSF-producing T cells into psoriatic skin.

Highlights

- Treg cells infiltrate into psoriasiform skin lesions
- Treg cells limit the exacerbation of skin inflammation and initiate disease remission
- GM-CSF^+CD4^+ T cells emerge in Treg-cell-depleted skin
- Neutralization of GM-CSF reverses exacerbated skin inflammation to wild-type levels

Hartwig et al., 2018, Cell Reports *25*, 3564–3572
December 26, 2018
https://doi.org/10.1016/j.celrep.2018.12.012

CellPress

OPEN ACCESS
CellPress

Cell Reports
Report

Regulatory T Cells Restrain Pathogenic T Helper Cells during Skin Inflammation

Tom Hartwig,[1,7] Pascale Zwicky,[1,7] Bettina Schreiner,[1,2] Nikhil Yawalkar,[3] Phil Cheng,[4] Alexander Navarini,[4] Reinhard Dummer,[4] Lukas Flatz,[5] Curdin Conrad,[6] Christoph Schlapbach,[3] and Burkhard Becher[1,8,*]
[1]Institute of Experimental Immunology, Department of Inflammation Research, University of Zurich, 8057 Zurich, Switzerland
[2]Department of Neurology, University Hospital Zurich, 8091 Zurich, Switzerland
[3]Department of Dermatology, Inselspital, University of Bern, 3010 Bern, Switzerland
[4]Department of Dermatology, University Hospital Zurich, 8091 Zurich, Switzerland
[5]Department of Dermatology and Allergology, Cantonal Hospital St. Gallen, St. Gallen, Switzerland
[6]Department of Dermatology, University Hospital CHUV, Lausanne 1011, Switzerland
[7]These authors contributed equally
[8]Lead Contact
*Correspondence: becher@immunology.uzh.ch
https://doi.org/10.1016/j.celrep.2018.12.012

SUMMARY

Psoriasis is a chronic relapsing, remitting interleukin (IL)-23/IL-17-driven skin disease mediated by the interplay of T cells and polymorphonuclear granulocytes. Although preclinical studies have provided insights into the mechanisms of disease initiation, the underpinnings of natural disease remission remain largely unknown. Here, we addressed the contribution of regulatory Foxp3$^+$ T cells (Treg cells) in psoriasiform skin inflammation and remission using the Aldara-skin inflammation model in combination with the inducible depletion of Foxp3$^+$ Treg cells. Loss of Treg cells exacerbated skin inflammation, but this did not involve increased $\gamma\delta$ T cell expansion or the local production of the psoriasis-associated cytokines IL-17A, IL-17F, and IL-22, which are the main driving forces of disease development. Instead, Treg cells suppressed the infiltration of granulocyte-macrophage colony-stimulating factor (GM-CSF)-producing CD4$^+$ T cells into the lesioned skin, and neutralizing GM-CSF in Treg cell-deficient mice reversed hyper-inflammation, resulting in disease regression. Therefore, we identified a non-redundant role of Treg cells restraining skin inflammation and mediating skin homeostasis.

INTRODUCTION

Psoriasis is one of the most common immune-mediated inflammatory disorders affecting 2%–3% of the world's population (Perera et al., 2012). To date, several forms of psoriasis have been described, including guttate, inverse, erythrodermic, arthritic, and plaque psoriasis (Menter et al., 2008). Plaque psoriasis, characterized by inflamed silver-white scaly skin, hyper-proliferation of keratinocytes, and dermal infiltrates of immune cells, is the most common form of psoriasis found in 85%–90% of patients (Nestle et al., 2009). Psoriasis patients suffer from a high disease burden and associated comorbidities, such as Crohn's disease (Gelfand et al., 2004; Nestle et al., 2009), type II diabetes (Yu et al., 2009; Shapiro et al., 2007), cardiovascular diseases (Perera et al., 2012; Davidovici et al., 2010), lymphoma (Gelfand et al., 2006), and depression (Kurd et al., 2010). Until today, the trigger causing this relapsing-remitting skin disease remains unknown. However, genetic predisposition in psoriasis-susceptible loci (PSORS) has been linked to psoriasis, including SNPs of the HLA.Cw6, interleukin-12b (IL-12b), or IL-23R loci (Nair et al., 2009). More recently, studies in human and mice unambiguously identified IL-23 and IL-17 as pathogenic drivers of this disease (Becher and Pantelyushin, 2012; Pantelyushin et al., 2012; Di Cesare et al., 2009). IL-17 is mainly produced by activated Th17 cells, $\gamma\delta$T cells, and type 3 innate lymphoid cells (ILCs) in response to dendritic cell (DC)-derived IL-1b and IL-23 (Becher and Pantelyushin, 2012; Baliwag et al., 2015).

One hallmark of psoriasis is the relapsing-remitting nature (Perera et al., 2012). Whereas dysregulated production of IL-23/IL-17 explains the relapse formation, the drivers behind disease remission remain elusive. Treg cells are a likely candidate for local control of inflammation and are found more frequently in the skin than in the circulation or other non-lymphoid tissues (Ali and Rosenblum, 2017). The majority of peripheral circulating human Treg cells express the skin homing receptor cutaneous lymphocyte antigen (CLA) and the chemokine receptor CCR6 (Hirahara et al., 2006). Their importance in preventing skin disease is most evident in patients suffering from the immunodysregulation polyendocrinopathy enteropathy x-linked (IPEX) syndrome caused by mutations in the Foxp3 gene, where cutaneous inflammation is highly common and occurs within the first months of life (Goudy et al., 2013; Halabi-Tawil et al., 2009). Dysfunctional or reduced Treg cells were also described in blood circulation and in psoriatic lesional skin in patients (Sugiyama et al., 2005; Keijsers et al., 2013), and Treg cells were found to be absent from newly formed acute psoriatic lesions shortly after disease initiation (Yun et al., 2010).

Although these data support the notion that Treg cells can restrain psoriatic skin pathology, the precise mechanism how Treg cells control psoriasiform skin inflammation is unknown. In order to address the functional role of Treg cells in skin inflammation, we specifically depleted Foxp3$^+$ Treg cells in the murine Aldara-induced model of psoriasis (van der Fits et al., 2009). Aldara-treated mice develop psoriasiform skin lesions mimicking most of the features of the human disease, and therapeutic agents, which are effective in the model, are equally effective in the human disease (Pantelyushin et al., 2012; Nestle et al., 2009). For the specific depletion of Foxp3$^+$ Treg cells, we utilized Foxp3$^{DTR/+}$ mice, in which the human diphtheria toxin receptor (DTR) is inserted into the 3′ UTR of the *Foxp3* locus. This allowed us to eliminate Foxp3$^+$ Treg cells at any time point by the injection of diphtheria toxin (DTx) (Kim et al., 2007). Using this approach, we found that Treg cells limit the exacerbation of local skin inflammation and initiate disease remission. Loss of Treg cells coincided with the emergence of pathogenic GM-CSF-producing CD4$^+$ T cells in the murine model of psoriasis and with the occurrence of GM-CSF in ipilimumab-induced skin rashes. Our study therefore indicates that Treg cells play a pivotal role in controlling psoriasiform skin inflammation and mediating skin homeostasis by restraining pathogenic effector cells.

RESULTS

Skin-Invading Foxp3$^+$ Treg Cells Control Aldara-Induced Skin Inflammation

The pathogenesis of Aldara-induced skin inflammation involves the emergence of various innate and adaptive immune cells. To analyze the skin lymphocyte compartment in psoriasiform lesions, we applied Aldara (5% imiquimod) topically to C57BL/6 mice (hereafter called wild-type [WT]) for eight days and harvested the treated skin at day nine. This was followed by single-cell cytometry combined with automated, algorithm-based t-distributed stochastic neighbor embedding (t-SNE) visualization and FlowSOM clustering of CD3$^+$ cells pre-gated on single, live, CD45$^+$ lymphocytes (Figure S1A). Clustering the most prominent lineage markers revealed six distinguishable cell populations in the skin (Figures 1A and S1B). Namely, skin-resident TCR$\gamma\delta^{high}$ cells (Vγ5$^+$ dendritic epidermal T cells [DETCs]), dermal Vγ4$^+$ (TCR$\gamma\delta^{int}$) and non-Vγ4$^+$ = Vγ6$^+$ cells (TCR$\gamma\delta^{int}$), Foxp3$^+$ T cells, CD4$^+$ T cells, and CD8$^+$ T cells. Aldara treatment induced a slight increase across all leukocytes in the skin. As expected (Cai et al., 2011; Pantelyushin et al., 2012), we observed a dramatic expansion of dermal Vγ4$^+$ cells and the accumulation of Treg cells in psoriatic skin (Figures 1A and 1B). More precisely, we found a five-fold increase of Foxp3$^+$ Treg cells in the Aldara-treated skin compared to untreated skin, accounting for up to 80 percent of the total population of skin-invading CD4$^+$ T cells (Figure 1B). To determine the role of Treg cells in the immunopathology of psoriasis, we treated Foxp3$^{DTR/+}$ mice with Aldara for eight consecutive days and injected 500 ng DTx on day four and six after Aldara treatment initiation (Figure 1C). After injection of DTx in either naive or Aldara-treated mice, Treg cells in the skin were almost completely absent, demonstrating that local Treg cell depletion was highly efficient (Figures 1D and 1E). Although skin inflammation in WT mice peaked at day five and regressed afterward, the disease of Treg-cell-depleted mice was dramatically exacerbated (3- to 4-fold), resulting in a steadily increasing thickening of the skin (Figure 1F). To further address whether Treg cells control the re-emergence of clinical symptoms after disease remission (hereafter referred as relapse), WT and Foxp3$^{DTR/+}$ mice were treated with Aldara for 21 days. In both groups, skin inflammation peaked at day 8 and declined afterward, despite continuous Aldara treatment. Treg cell depletion in recovering mice led to a relapse of psoriasiform skin lesions (Figure S1C). Therefore, we conclude that Treg cells play a critical role in controlling psoriasiform inflammation.

Emergence of $\alpha\beta$ T Cells and Phagocytes in Psoriasiform Skin Lesions upon Treg Cell Loss

Lesional skin of psoriasis patients is invaded by several immune cells, including T cells and polymorphonuclear and mononuclear phagocytes (Nestle et al., 2009). To better understand how Treg cells control skin inflammation, we analyzed the cellular composition of the skin at the peak of psoriasiform inflammation in the presence or absence of Treg cells by flow cytometry. We again used t-SNE visualization and FlowSOM clustering to analyze the overall T cell infiltrates depending on their similarity in the expression of lineage-specific markers. The five discernible clusters were TCR$\gamma\delta^{high}$ (DETCs), Vγ4, Vγ6, $\alpha\beta$ T cells, and Treg cells (Figure 2A). To define cell populations based on parameter expression heatmaps, we followed similar analysis workflow as shown in Figure S1B. As previously reported, Vγ4$^+$ T cells are the source of IL-17 and IL-22, and as such, the main drivers of Aldara-induced skin inflammation and $\alpha\beta$ T cells are (1) not critical for disease development and (2) almost absent from the lesional skin (Pantelyushin et al., 2012; Hartwig et al., 2015). We thus suspected that Treg cells might control the pathogenic signature cytokines and/or Vγ4$^+$T17 cell infiltration into the skin. However, Vγ4$^+$ T cells were not elevated in Treg cell-deficient mice showing that Treg cells did not directly control the IL-17-producing pathogenic Vγ4$^+$ T cells (Figure 2B). In contrast, we observed the local accumulation of CD4$^+$ and CD8$^+$ T cells in Treg-cell-depleted mice, compared to control groups (Figures 2A and 2B). Of note, Treg cell depletion *per se* did not alter the composition of the skin leukocyte compartment when the mice were not challenged with Aldara (Figures 2A and 2B).

We next focused on the myeloid compartment and identified five distinct clusters, including neutrophils, Ly6C$^+$ monocytes, monocyte-derived cells (MdCs) and macrophages, Langerhans cells (LCs), and plasmacytoid dendritic cells (pDCs) (Figure 2C). Quantification of myeloid subsets showed that neutrophils and MdCs were the dominant cell types infiltrating the skin in Aldara-treated Treg cell–deficient mice (Figures 2C and 2D). We also analyzed the composition of leukocytes within the skin draining lymph nodes (dLN) and found a relative increase in all populations led by CD19$^+$ B cells and CD4$^+$ and CD8$^+$ T cells upon Treg cells depletion (Figure S2A). More detailed phenotyping of T cells in the dLN showed that the vast majority of CD4 T cells are CD44$^+$CD62L$^-$ effector memory T cells in Treg cell-deficient mice, whereas CD8 T cells were CD44$^+$CD62L$^+$ (Figure S2B). CD8 T cells also upregulated the early activation antigen CD69 (Figure S2C). Both CD4 and CD8 T cell compartments were positive for Ki-67, indicative of proliferation (Figure S2D). Together, our data suggest that Treg cells do not control the initiation of

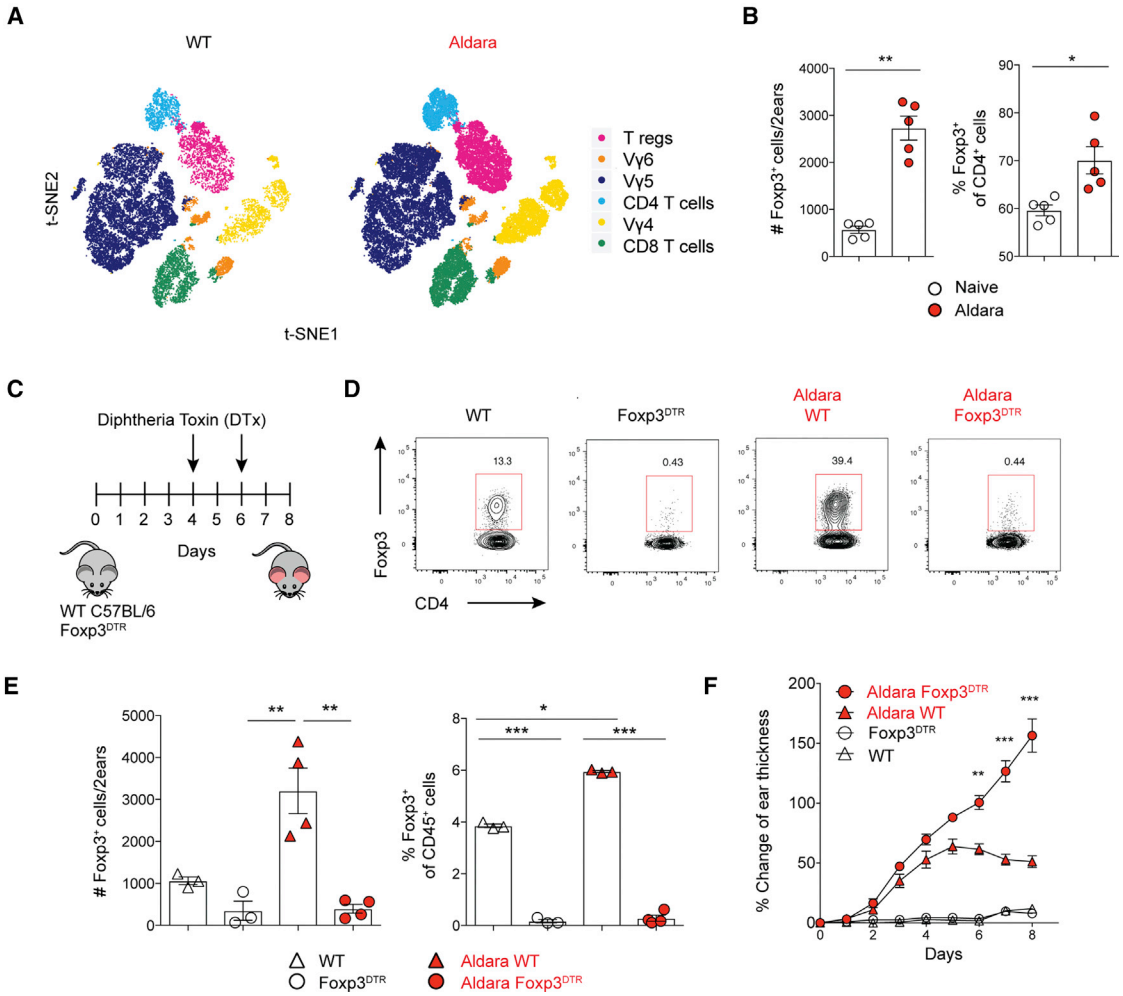

Figure 1. Skin-Invading Foxp3⁺ Treg Cells Control Aldara-Induced Skin Inflammation

(A and B) Ears of WT mice were treated topically with Aldara for eight consecutive days, and skin lymphocytes were analyzed by flow cytometry on day nine.

(A) $CD45^+CD3^+$ cells were used for algorithm-based t-SNE visualization and FlowSOM clustering based on their expression of T-cell-specific lineage markers (see also Figure S1B).

(B) Bar charts show total numbers (left) and percentages (right) of $Foxp3^+CD3^+$ cells from naive and Aldara-treated mice.

(C–F) *Foxp3*$^{DTR/+}$ and WT mice were treated daily with Aldara (red) on the ears for eight days or were left untreated (black), and skin lymphocytes were analyzed by flow cytometry on day nine. All groups were injected intraperitoneally (i.p.) with 500 ng DTx on day four and day six after Aldara treatment initiation.

(C) Schematic illustration of the experimental setup.

(D) Representative contour plots show the percentage of $CD4^+Foxp3^+$ T cells (pre-gated on $CD45^+CD3^+$ cells).

(E) Bar graphs show the total cell numbers (left) and frequencies (right) of $CD4^+Foxp3^+$ T cells.

(F) Kinetics of skin inflammation depicted as percentage increase in ear thickness. Two-way ANOVA with Bonferroni's posttest is shown.

In (A), (B), and (D)–(F), displayed results are representative of three independent experiments (n = 3–5). In (B) and (E), data are shown as mean ± SEM two-tailed Student's t test. *$p < 0.05$; **$p < 0.01$; ***$p < 0.001$. DTx, diphtheria toxin; WT, wild-type.

See also Figure S1.

psoriasiform lesions or the emergence of γδT17 cells but instead limit the ability of αβ T cells to invade and expand in the lesional skin and dLNs.

Treg Cells Prevent Expansion of Pathogenic GM-CSF-Producing $CD4^+$ T Cells in the Skin

Given the importance of IL-17A, IL-17F, IL-22, and tumor necrosis factor (TNF) in the formation of psoriasiform lesions, we were surprised to find no dramatic changes in these cytokines in Aldara-treated mice upon Treg cell loss (Figure 3A). Instead, we found the strongest change of cytokine expression among $CD3^+$ T cells to be GM-CSF (80-fold; Figure 3A). GM-CSF was mainly produced by $CD45^+$ cells and among them chiefly by $CD4^+$ T cells (Figures 3B–3D). These GM-CSF^+ $CD4^+$ T cells did not co-produce the psoriasis-associated cytokines IL-22, IL-17A, and IL-17F (Figure S3A) but were positive for IL-23R (Figure S3B). We further analyzed common cytokines driving GM-CSF production in T cells and found elevated levels of

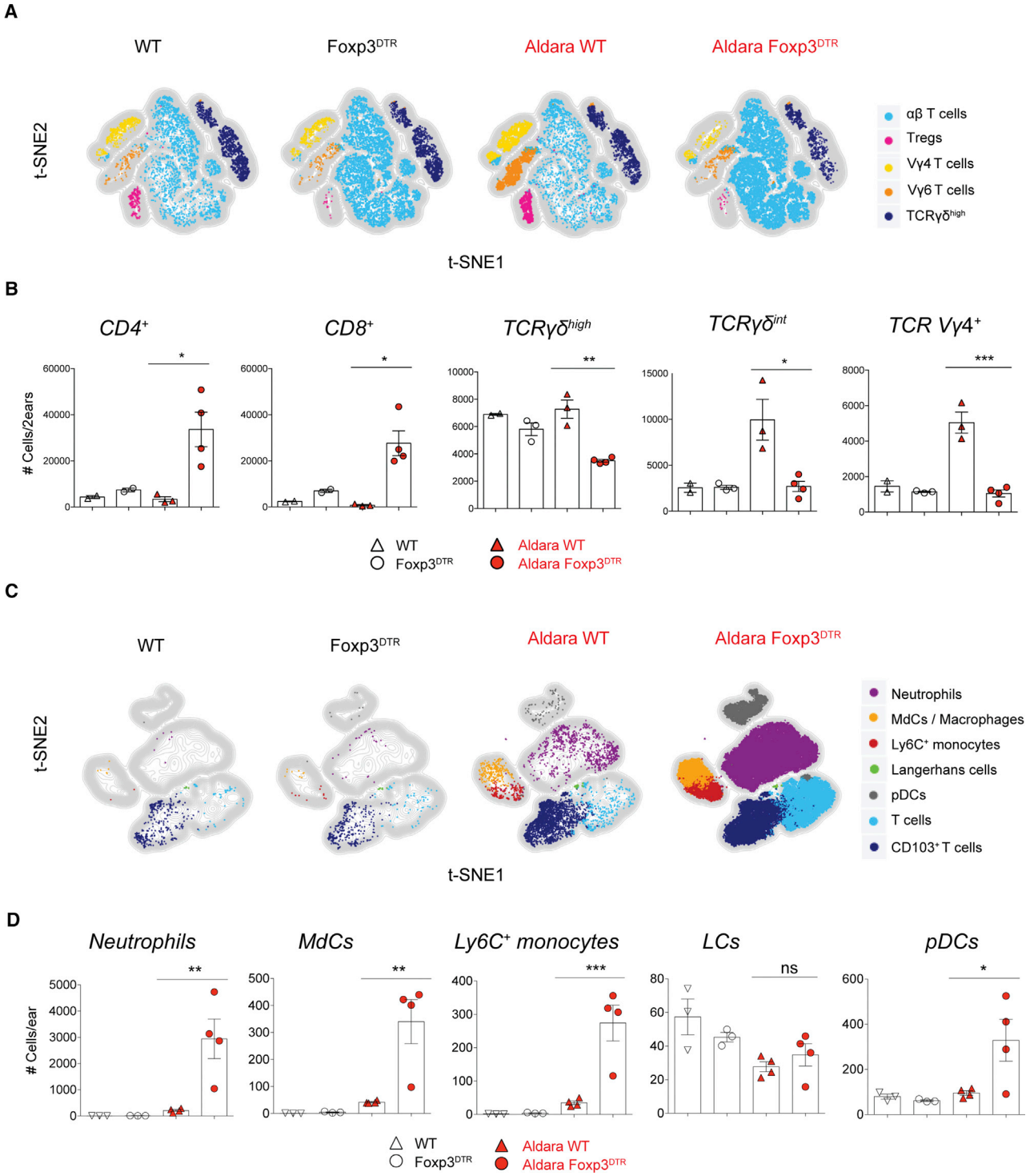

Figure 2. Accumulation of αβ T Cells and Phagocytes in Psoriasiform Skin Lesions upon Treg Cell Loss

(A–D) Foxp3$^{DTR/+}$ and WT mice were challenged with Aldara on their ears for eight consecutive days (red) or were left untreated (black). 500 ng DTx was injected i.p. on day four and six after Aldara treatment initiation. Skin lymphocytes were analyzed on day nine by flow cytometry.

(A) CD45$^+$CD3$^+$ cells were visualized by t-SNE and clustered by FlowSOM depending on their similarity in the expression of lineage-specific markers.

(B) Total cell numbers (±SEM) of CD4$^+$Foxp3$^-$, CD8$^+$, TCRγδ^{high}, TCRγδ^{int}, and Vγ4$^+$ cells.

(C) CD45$^+$CD19$^-$ cells were used for t-SNE visualization and FlowSOM clustering.

(D) Total cell numbers (±SEM) of neutrophils, MdCs, Ly6C$^+$ monocytes, LCs, and pDCs.

(legend continued on next page)

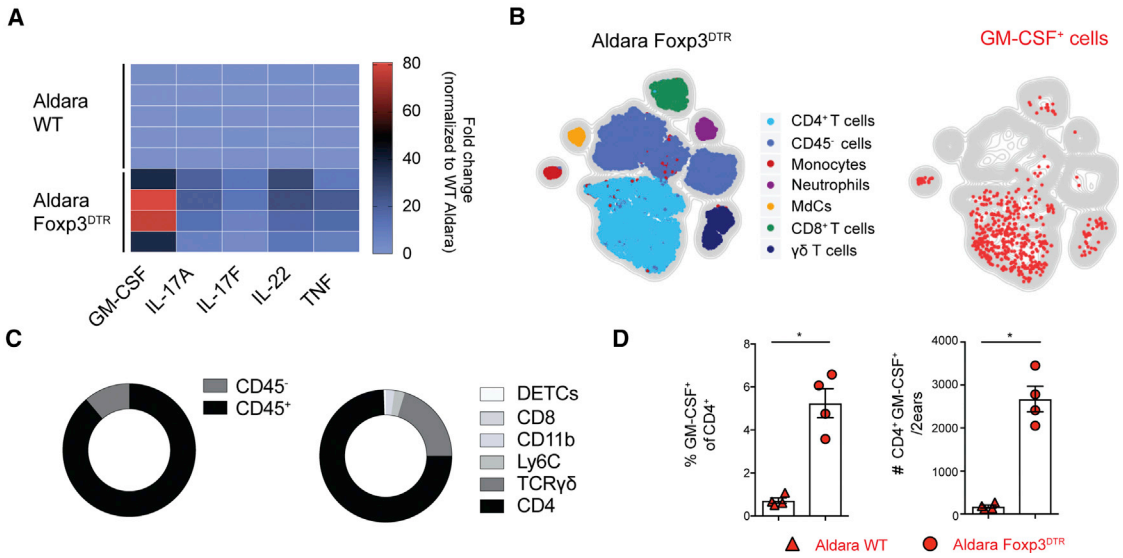

Figure 3. Treg Cells Prevent Expansion of Pathogenic GM-CSF-Producing CD4$^+$ T Cells in the Skin

(A–D) Foxp3$^{DTR/+}$ and WT mice were treated with Aldara daily on the ear for eight days. On day four and six, both groups were injected i.p. with 500 ng DTx. Flow cytometric analysis of skin lymphocytes was performed on day nine.

(A) Heatmap showing fold change in cytokine expression of CD3$^+$ cells normalized to Aldara-treated WT mice.

(B) Total skin cells (left) or GM-CSF-producing cells (right) were visualized using t-SNE algorithm and clustered by FlowSOM depending on their similarity in the expression of linage-specific markers (left).

(C) Donut charts showing percentages of GM-CSF-expressing cells from Aldara- and DTx-treated Foxp3$^{DTR/+}$ mice. CD45$^+$ and CD45$^-$ cells (left) and DETCs, CD8$^+$, CD11b$^+$, Ly6C$^+$, TCR$\gamma\delta^+$, and CD4$^+$ cells (right) are shown.

(D) Percentages of GM-CSF-producing CD4$^+$ T cells from the LN (left) and total cell numbers from the skin (right; ± SEM).

In (A)–(D), one representative of three independent experiments (n = 3–5) is shown.

Two-tailed Student's t test is shown. *p < 0.05; **p < 0.01; ***p < 0.001. DETCs, dendritic epidermal T cells.

See also Figure S3.

pro-IL-1β but failed to observe major changes in the expression of *Il23a* or *Il12a* (Figure S3C). We identified skin-invading Ly6-C^{high} monocytes and neutrophils as the chief producers of pro-IL-1β in Aldara-treated Treg cell-deficient mice (Figure S3D).

To determine whether the Treg cell–dependent control of GM-CSF-producing T cells is the reason for the observed hyper-inflammation in Aldara-treated Treg cell-deficient mice, we employed either a neutralizing anti-GM-CSF antibody or GM-CSF-deficient mice. Foxp3$^{DTR/+}$ mice were injected with 300 μg of anti-GM-CSF antibody (Ab) every second day until day six after Aldara treatment start (Figure 4A). Neutralization or loss of GM-CSF in Treg-cell-depleted mice reversed skin inflammation to WT levels (Figure 4B). Importantly, GM-CSF neutralization did not stop the accumulation of GM-CSF-producing T helper (TH) cells in the skin of Treg-cell-depleted mice (Figure 4C). This is not surprising because T cells generally do not express the receptor complex for sensing GM-CSF. Also, this indicates that GM-CSF$^+$ TH cells in the skin are directly controlled by Treg cells and that the elevated frequency of GM-CSF$^+$ TH cells is not the result of enhanced skin inflammation *per se*. Histological analysis revealed that the increased epidermal thickness found in Treg-cell-depleted mice was reduced in the absence of *csf2* (Figures 4D and 4E). Our data demonstrate that Treg cells control the occurrence of hyper-active pathogenic effector T cells, which produce GM-CSF and subsequent immunopathology.

To support our findings of GM-CSF appearance following Treg cell depletion in mice, also in human skin, we analyzed GM-CSF levels of ipilimumab (α-CTLA-4 monoclonal antibody [mAb])-induced skin rashes. Treatment of melanoma patients with ipilimumab (IP) can cause severe skin manifestations and pathologies by neutralization of Treg cells (Bertrand et al., 2015; Romano et al., 2015). Comparing ipilimumab-induced flares with skin from healthy donors (HC), we observed higher levels of *Csf2* mRNA transcripts in the skin from ipilimumab (Figures S4A and S4B), suggesting that Treg cells may have a universal role in maintaining skin homeostasis and that conversely perturbations of Treg cells could initiate skin pathologies.

DISCUSSION

Psoriasis has been considered as a Th1-driven skin disease for almost 30 years. After the discovery of pathogenic

Two-tailed Student's t test was used in (B) and (D). *p < 0.05; **p < 0.01; ***p < 0.001.

In (A)–(D), a representative experiment (n = 2–4) of three independent experiments is shown. LCs, Langerhans cells; MdCs, monocyte-derived cells; pDCs, plasmacytoid dendritic cells.

See also Figure S2.

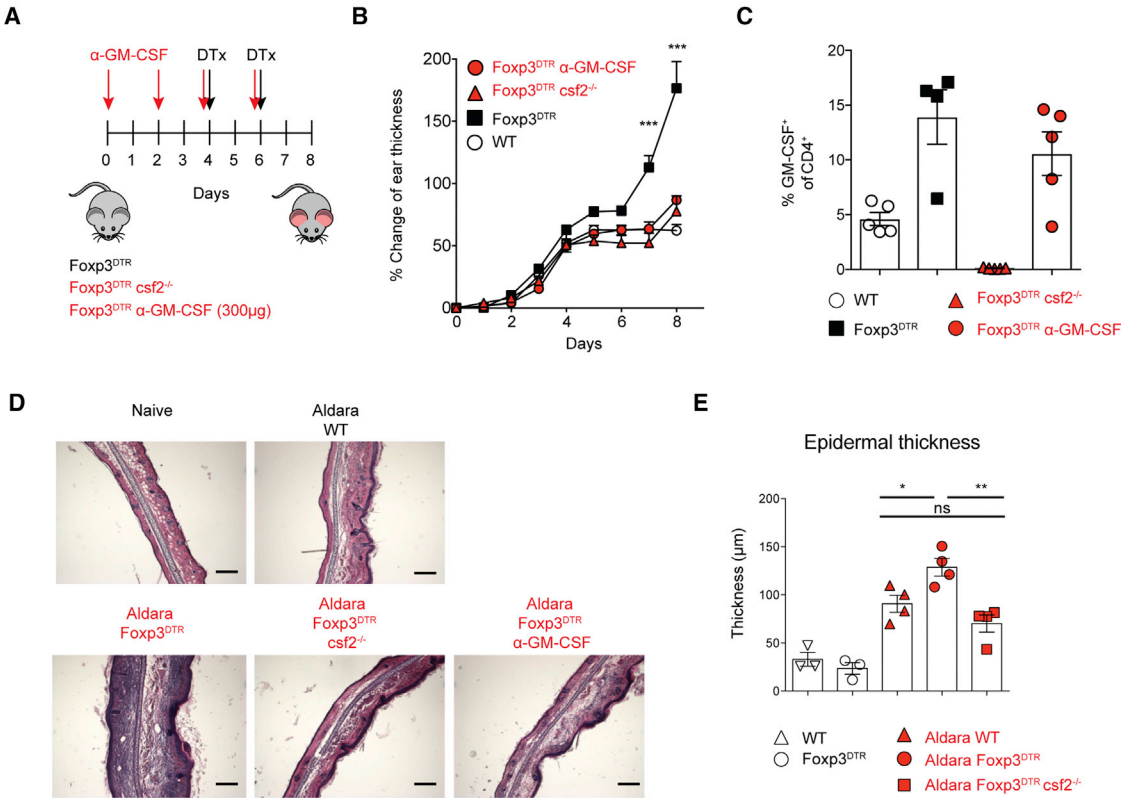

Figure 4. Neutralizing GM-CSF in Treg Cell-Deficient Mice Reverses Hyper-inflammation

(A–E) WT, Foxp3$^{DTR/+}$, and Foxp3$^{DTR/+}$*Csf2*$^{-/-}$ mice were treated topically with Aldara on their ears for eight consecutive days, and DTx was injected i.p. on days four and six. Additionally, one Foxp3$^{DTR/+}$ group was injected i.p. with anti-GM-CSF antibody every second day starting at day 0.

(A) Schematic illustration of the experimental setup.

(B) Kinetics of skin inflammation depicted as percentage increase in ear thickness (±SEM); two-way ANOVA with Bonferroni's posttest.

(C) Percentage (±SEM) of GM-CSF-expressing CD4$^+$ T cells (pre-gated on CD45$^+$CD11b$^-$ lymphocytes) analyzed by flow cytometry on day nine.

(D and E) On day nine, ears were Hepes-glutamic acid buffer-mediated organic solvent protection effect (HOPE) fixed and sections were stained with H&E.

(D) Representative images. Scale bars 220 μm.

(E) Bar graph showing epidermal thickening measured on images of H&E stainings.

In (A)–(C), one representative of three independent experiments (n = 3–5) is shown. In (D) and (E), one representative of two independent experiments (n = 3–4) is shown.

Two-tailed Student's t test is shown. *p < 0.05; **p < 0.01; ***p < 0.001. ns, not significant.

IL-17-producing T cells in psoriasis, this paradigm shifted completely and new therapeutic approaches against the IL-23-IL-17 pathway were successfully introduced (Nast et al., 2012; Langley et al., 2014). To date, these therapies are mostly directed against the pathogenic drivers of the disease, disregarding potential pathways regulating the disease chronification. Although Treg cells maintain immune tolerance through various well-characterized mechanisms (Walker, 2013; Sakaguchi et al., 2008), the mechanisms and dynamics by which Treg cells control ongoing psoriasiform skin inflammation are still not completely understood. To address how Treg cells contribute to skin inflammation, we utilized Foxp3^{DTR} mice to eliminate Treg cells in a murine model of psoriasis. We found that Treg cells accumulate and control the exacerbation of skin inflammation by restraining pathogenic GM-CSF-producing CD4$^+$ T cells. Even though the IL-23-IL-17 axis is clearly driving the pathogenesis of psoriasis, the role of dysregulated GM-CSF expression in the skin is still a matter of debate. Pointing toward the contribution of GM-CSF in disease development, recombinant GM-CSF therapy for the treatment of neutropenia following chemotherapy led to relapsing and exacerbating psoriasis flares in breast cancer patients (Cho et al., 1998). Accordingly, a recent study found neutralization of GM-CSF to reduce skin pathology in Aldara-driven psoriasis (Scholz et al., 2017). Nonetheless, a recent phase II clinical trial showed no benefit of the use of anti-GM-CSF Abs (namilumab) in plaque psoriasis (https://clinicaltrials.gov/: NCT02129777; Papp et al., 2018). Of note, the penetration of Abs into skin is much lower than into joints of rheumatoid arthritis patients, in which namilumab demonstrated a high efficacy (Choy et al., 2000; Papp et al., 2018; https://clinicaltrials.gov/: NCT023790091).

Importantly, we found exacerbated skin inflammation and elevated GM-CSF levels only in the absence of Treg cells, but not in psoriasiform inflammation of Treg cell–sufficient WT mice. Neutralization of GM-CSF in Treg cell-deficient mice

reversed hyper-inflammation to WT levels, suggesting that GM-CSF is not important for disease initiation but is driving the aggravation of established skin lesions. Given that GM-CSF is part of a cytokine network, it is likely that targeting of GM-CSF further changes several downstream cytokines involved in Treg cell–regulated inflammation.

The fact that GM-CSF is upregulated in human skin rashes induced by α-CTLA4 supports a general function of Treg cells controlling skin inflammation and suggests that Treg cells are vital in maintaining skin homeostasis. GM-CSF has emerged as an essential communication conduit between inflammatory T cells and tissue-invading phagocytes (Becher et al., 2016, 2017). Here, psoriasiform skin lesions were preferentially invaded by neutrophils and monocytes, both well-described cell types responding to GM-CSF (Ko et al., 2014; Kroenke et al., 2010; Croxford et al., 2015).

So far, we can only speculate by which molecular mechanism Treg cells control pathogenic skin $CD4^+$ T cells. It is very likely that the loss of Treg cells licenses skin-resident DCs to initiate their pathogenic program, including exacerbated secretion of cytokines. In support of this idea, we observed the enhanced delivery of IL-1β into the lesioned skin of mice in which Treg cells have been depleted. IL-1β in turn is well established to induce GM-CSF expression in T cells (El-Behi et al., 2011). In other studies, Treg cells have been shown to limit DC functions and thus T cell responses by CTLA-4 and Lag3 in a contact-dependent manner (Vignali et al., 2008). However, effector T cells can also be directly controlled by inhibitory Treg cell–derived cytokines, such as IL-10 and transforming growth factor β (TGF-β). Another possibility of accumulated effector T cell in the skin upon Treg cell depletion is the excess of IL-2 at the inflammation site. IL-2 directly induces GM-CSF expression (Hartmann et al., 2014), and Treg cells capture IL-2, thereby reducing the proliferation of other T cells.

In summary, we identified a pathway by which Treg cells suppress the exacerbation of psoriasiform inflammation through the control of pathogenic GM-CSF-producing αβ T cells, suggesting that this interplay contributes to the relapsing-remitting nature of the disease.

STAR★METHODS

Detailed methods are provided in the online version of this paper and include the following:

- KEY RESOURCES TABLE
- CONTACT FOR REAGENT AND RESOURCE SHARING
- EXPERIMENTAL MODEL AND SUBJECT DETAILS
  - Animal models
  - Human studies
- METHOD DETAILS
  - *In vivo* treatments
  - Tissue processing
  - Flow Cytometry
  - Quantitative RT-PCR (qRT-PCR)
  - Histology
  - t-SNE visualization
- QUANTIFICATION AND STATISTICAL ANALYSIS

SUPPLEMENTAL INFORMATION

Supplemental Information includes four figures and one table and can be found with this article online at https://doi.org/10.1016/j.celrep.2018.12.012.

ACKNOWLEDGMENTS

This study was supported by grants to B.B. from the Swiss National Science Foundation (310030_146130, 316030_150768, and 310030_170320), the European Union (FP7 ITN NeuroKine, FP7 Project ATECT), and the University Priority Project Translational Cancer Research. We further thank Sarah Mundt for manuscript preparation; Anto Pavlovic, Mirjam Lutz, Ana Amorim, and Claudia Haftmann for technical assistance; and the Cytometry Facility (University of Zurich) for technical support.

AUTHOR CONTRIBUTIONS

T.H. and P.Z. designed and performed experiments and data analysis. B.S. performed immunohistochemistry. C.S., N.Y., P.C., R.D., L.F., C.C., and A.N. provided human skin samples from ipilimumab-treated patients and healthy donors. B.B. supervised and financed the study. T.H., P.Z., and B.B. wrote the manuscript.

DECLARATION OF INTERESTS

R.D. has intermittent, project-focused consulting and/or advisory relationships with Novartis, Merck Sharp & Dhome (MSD), Bristol-Myers Squibb (BMS), Roche, Amgen, Takeda, Pierre Fabre, and Sun Pharma outside the submitted work.

Received: June 4, 2018
Revised: November 13, 2018
Accepted: December 3, 2018
Published: December 26, 2018

REFERENCES

Ali, N., and Rosenblum, M.D. (2017). Regulatory T cells in skin. Immunology *152*, 372–381.

Amir, A.D., Davis, K.L., Tadmor, M.D., Simonds, E.F., Levine, J.H., Bendall, S.C., Shenfeld, D.K., Krishnaswamy, S., Nolan, G.P., and Pe'er, D. (2013). viSNE enables visualization of high dimensional single-cell data and reveals phenotypic heterogeneity of leukemia. Nat. Biotechnol. *31*, 545–552.

Baliwag, J., Barnes, D.H., and Johnston, A. (2015). Cytokines in psoriasis. Cytokine *73*, 342–350.

Becher, B., and Pantelyushin, S. (2012). Hiding under the skin: interleukin-17-producing γδ T cells go under the skin? Nat. Med. *18*, 1748–1750.

Becher, B., Tugues, S., and Greter, M. (2016). GM-CSF: From Growth Factor to Central Mediator of Tissue Inflammation. Immunity *45*, 963–973.

Becher, B., Spath, S., and Goverman, J. (2017). Cytokine networks in neuroinflammation. Nat. Rev. Immunol. *17*, 49–59.

Bertrand, A., Kostine, M., Barnetche, T., Truchetet, M.E., and Schaeverbeke, T. (2015). Immune related adverse events associated with anti-CTLA-4 antibodies: systematic review and meta-analysis. BMC Med. *13*, 211.

Cai, Y., Shen, X., Ding, C., Qi, C., Li, K., Li, X., Jala, V.R., Zhang, H.G., Wang, T., Zheng, J., et al. (2011). Pivotal role of dermal IL-17-producing γδ t cells in skin inflammation. Immunity *35*, 596–610.

Cho, S.G., Park, Y.M., Moon, H., Kim, K.M., Bae, S.S., Kim, G.B., Cho, H.S., Kim, C.C., and Lee, K.S. (1998). Psoriasiform eruption triggered by recombinant granulocyte-macrophage colony stimulating factor (rGM-CSF) and exacerbated by granulocyte colony stimulating factor (rG-CSF) in a patient with breast cancer. J. Korean Med. Sci. *13*, 685–688.

Choy, E.H., Connolly, D.J., Rapson, N., Jeal, S., Brown, J.C., Kingsley, G.H., Panayi, G.S., and Johnston, J.M. (2000). Pharmacokinetic, pharmacodynamic and clinical effects of a humanized IgG1 anti-CD4 monoclonal antibody in the

peripheral blood and synovial fluid of rheumatoid arthritis patients. Rheumatology (Oxford) *39*, 1139–1146.

Croxford, A.L., Lanzinger, M., Hartmann, F.J., Schreiner, B., Mair, F., Pelczar, P., Clausen, B.E., Jung, S., Greter, M., and Becher, B. (2015). The Cytokine GM-CSF Drives the Inflammatory Signature of CCR2+ Monocytes and Licenses Autoimmunity. Immunity *43*, 502–514.

Davidovici, B.B., Sattar, N., Prinz, J., Puig, L., Emery, P., Barker, J.N., van de Kerkhof, P., Ståhle, M., Nestle, F.O., Girolomoni, G., and Krueger, J.G. (2010). Psoriasis and systemic inflammatory diseases: potential mechanistic links between skin disease and co-morbid conditions. J. Invest. Dermatol. *130*, 1785–1796.

Di Cesare, A., Di Meglio, P., and Nestle, F.O. (2009). The IL-23/Th17 axis in the immunopathogenesis of psoriasis. J. Invest. Dermatol. *129*, 1339–1350.

Dranoff, G., Crawford, A.D., Sadelain, M., Ream, B., Rashid, A., Bronson, R.T., Dickersin, G.R., Bachurski, C.J., Mark, E.L., Whitsett, J.A., et al. (1994). Involvement of granulocyte-macrophage colony-stimulating factor in pulmonary homeostasis. Science *264*, 713–716.

El-Behi, M., Ciric, B., Dai, H., Yan, Y., Cullimore, M., Safavi, F., Zhang, G.X., Dittel, B.N., and Rostami, A. (2011). The encephalitogenicity of TH17 cells is dependent on IL-1- and IL-23-induced production of the cytokine GM-CSF. Nat. Immunol. *12*, 568–575.

Gelfand, J.M., Feldman, S.R., Stern, R.S., Thomas, J., Rolstad, T., and Margolis, D.J. (2004). Determinants of quality of life in patients with psoriasis: a study from the US population. J. Am. Acad. Dermatol. *51*, 704–708.

Gelfand, J.M., Shin, D.B., Neimann, A.L., Wang, X., Margolis, D.J., and Troxel, A.B. (2006). The risk of lymphoma in patients with psoriasis. J. Invest. Dermatol. *126*, 2194–2201.

Goudy, K., Aydin, D., Barzaghi, F., Gambineri, E., Vignoli, M., Ciullini Mannurita, S., Doglioni, C., Ponzoni, M., Cicalese, M.P., Assanelli, A., et al. (2013). Human IL2RA null mutation mediates immunodeficiency with lymphoproliferation and autoimmunity. Clin. Immunol. *146*, 248–261.

Halabi-Tawil, M., Ruemmele, F.M., Fraitag, S., Rieux-Laucat, F., Neven, B., Brousse, N., De Prost, Y., Fischer, A., Goulet, O., and Bodemer, C. (2009). Cutaneous manifestations of immune dysregulation, polyendocrinopathy, enteropathy, X-linked (IPEX) syndrome. Br. J. Dermatol. *160*, 645–651.

Hartmann, F.J., Khademi, M., Aram, J., Ammann, S., Kockum, I., Constantinescu, C., Gran, B., Piehl, F., Olsson, T., Codarri, L., et al. (2014). Multiple sclerosis-associated IL2RA polymorphism controls GM-CSF production in human T. Nat. Commun. *5*, 1–10.

Hartmann, F.J., Bernard-Valnet, R., Quériault, C., Mrdjen, D., Weber, L.M., Galli, E., Krieg, C., Robinson, M.D., Nguyen, X.H., Dauvilliers, Y., et al. (2016). High-dimensional single-cell analysis reveals the immune signature of narcolepsy. J. Exp. Med. *213*, 2621–2633.

Hartwig, T., Pantelyushin, S., Croxford, A.L., Kulig, P., and Becher, B. (2015). Dermal IL-17-producing γδ T cells establish long-lived memory in the skin. Eur. J. Immunol. *45*, 3022–3033.

Hirahara, K., Liu, L., Clark, R.A., Yamanaka, K., Fuhlbrigge, R.C., and Kupper, T.S. (2006). The majority of human peripheral blood CD4+CD25highFoxp3+ regulatory T cells bear functional skin-homing receptors. J. Immunol. *177*, 4488–4494.

Keijsers, R.R., van der Velden, H.M., van Erp, P.E., de Boer-van Huizen, R.T., Joosten, I., Koenen, H.J., and van de Kerkhof, P.C. (2013). Balance of Treg vs. T-helper cells in the transition from symptomless to lesional psoriatic skin. Br. J. Dermatol. *168*, 1294–1302.

Kim, J.M., Rasmussen, J.P., and Rudensky, A.Y. (2007). Regulatory T cells prevent catastrophic autoimmunity throughout the lifespan of mice. Nat. Immunol. *8*, 191–197.

Ko, H.J., Brady, J.L., Ryg-Cornejo, V., Hansen, D.S., Vremec, D., Shortman, K., Zhan, Y., and Lew, A.M. (2014). GM-CSF-responsive monocyte-derived dendritic cells are pivotal in Th17 pathogenesis. J. Immunol. *192*, 2202–2209.

Kroenke, M.A., Chensue, S.W., and Segal, B.M. (2010). EAE mediated by a non-IFN-γ/non-IL-17 pathway. Eur. J. Immunol. *40*, 2340–2348.

Kurd, S.K., Troxel, A.B., Crits-Christoph, P., and Gelfand, J.M. (2010). The risk of depression, anxiety, and suicidality in patients with psoriasis: a population-based cohort study. Arch. Dermatol. *146*, 891–895.

Langley, R.G., Elewski, B.E., Lebwohl, M., Reich, K., Griffiths, C.E., Papp, K., Puig, L., Nakagawa, H., Spelman, L., Sigurgeirsson, B., et al.; ERASURE Study Group; FIXTURE Study Group (2014). Secukinumab in plaque psoriasis–results of two phase 3 trials. N. Engl. J. Med. *371*, 326–338.

van der Maaten, L., and Hinton, G. (2008). Visualizing data using t-SNE. J. Mach. Learn. Res. *9*, 2579–2605.

Menter, A., Gottlieb, A., Feldman, S.R., Van Voorhees, A.S., Leonardi, C.L., Gordon, K.B., Lebwohl, M., Koo, J.Y., Elmets, C.A., Korman, N.J., et al. (2008). Guidelines of care for the management of psoriasis and psoriatic arthritis: section 1. Overview of psoriasis and guidelines of care for the treatment of psoriasis with biologics. J. Am. Acad. Dermatol. *58*, 826–850.

Nair, R.P., Duffin, K.C., Helms, C., Ding, J., Stuart, P.E., Goldgar, D., Gudjonsson, J.E., Li, Y., Tejasvi, T., Feng, B.J., et al.; Collaborative Association Study of Psoriasis (2009). Genome-wide scan reveals association of psoriasis with IL-23 and NF-kappaB pathways. Nat. Genet. *41*, 199–204.

Nast, A., Boehncke, W.H., Mrowietz, U., Ockenfels, H.M., Philipp, S., Reich, K., Rosenbach, T., Sammain, A., Schlaeger, M., Sebastian, M., et al.; Deutsche Dermatologische Gesellschaft (DDG); Berufsverband Deutscher Dermatologen (BVDD) (2012). S3 - Guidelines on the treatment of psoriasis vulgaris (English version). Update. J. Dtsch. Dermatol. Ges. *10* (*Suppl 2*), S1–S95.

Nestle, F.O., Kaplan, D.H., and Barker, J. (2009). Psoriasis. N. Engl. J. Med. *361*, 496–509.

Pantelyushin, S., Haak, S., Ingold, B., Kulig, P., Heppner, F.L., Navarini, A.A., and Becher, B. (2012). Rorγt+ innate lymphocytes and γδ T cells initiate psoriasiform plaque formation in mice. J. Clin. Invest. *122*, 2252–2256.

Papp, K.A., Gooderham, M., Jenkins, R., Vender, R., Szepietowski, J.C., Wagner, T., Hunt, B., and Souberbielle, B.; Neptune Investigators (2018). Granulocyte-macrophage colony-stimulating factor (GM-CSF) as a therapeutic target in psoriasis: randomised, controlled investigation using namilumab, a specific human anti-GM-CSF monoclonal antibody. Br. J. Dermatol. Published online September 12, 2018. https://doi.org/10.1111/bjd.17195.

Perera, G.K., Di Meglio, P., and Nestle, F.O. (2012). Psoriasis. Annu. Rev. Pathol. *7*, 385–422.

Romano, E., Kusio-Kobialka, M., Foukas, P.G., Baumgaertner, P., Meyer, C., Ballabeni, P., Michielin, O., Weide, B., Romero, P., and Speiser, D.E. (2015). Ipilimumab-dependent cell-mediated cytotoxicity of regulatory T cells ex vivo by nonclassical monocytes in melanoma patients. Proc. Natl. Acad. Sci. USA *112*, 6140–6145.

Sakaguchi, S., Yamaguchi, T., Nomura, T., and Ono, M. (2008). Regulatory T cells and immune tolerance. Cell *133*, 775–787.

Scholz, T., Weigert, A., Brüne, B., Sadik, C.D., Böhm, B., and Burkhardt, H. (2017). GM-CSF in murine psoriasiform dermatitis: redundant and pathogenic roles uncovered by antibody-induced neutralization and genetic deficiency. PLoS ONE *12*, e0182646.

Shapiro, J., Cohen, A.D., David, M., Hodak, E., Chodik, G., Viner, A., Kremer, E., and Heymann, A. (2007). The association between psoriasis, diabetes mellitus, and atherosclerosis in Israel: a case-control study. J. Am. Acad. Dermatol. *56*, 629–634.

Streeck, H., Cohen, K.W., Jolin, J.S., Brockman, M.A., Meier, A., Power, K.A., Waring, M.T., Alter, G., and Altfeld, M. (2008). Rapid ex vivo isolation and long-term culture of human Th17 cells. J. Immunol. Methods *333*, 115–125.

Sugiyama, H., Gyulai, R., Toichi, E., Garaczi, E., Shimada, S., Stevens, S.R., McCormick, T.S., and Cooper, K.D. (2005). Dysfunctional blood and target tissue CD4+CD25high regulatory T cells in psoriasis: mechanism underlying unrestrained pathogenic effector T cell proliferation. J. Immunol. *174*, 164–173.

van der Fits, L., Mourits, S., Voerman, J.S., Kant, M., Boon, L., Laman, J.D., Cornelissen, F., Mus, A.M., Florencia, E., Prens, E.P., and Lubberts, E. (2009). Imiquimod-induced psoriasis-like skin inflammation in mice is mediated via the IL-23/IL-17 axis. J. Immunol. *182*, 5836–5845.

Van Gassen, S., Callebaut, B., Van Helden, M.J., Lambrecht, B.N., Demeester, P., Dhaene, T., and Saeys, Y. (2015). FlowSOM: Using self-organizing maps for visualization and interpretation of cytometry data. Cytometry A *87*, 636–645.

Vignali, D.A., Collison, L.W., and Workman, C.J. (2008). How regulatory T cells work. Nat. Rev. Immunol. *8*, 523–532.

Walker, L.S. (2013). Treg and CTLA-4: two intertwining pathways to immune tolerance. J. Autoimmun. *45*, 49–57.

Yu, A.P., Tang, J., Xie, J., Wu, E.Q., Gupta, S.R., Bao, Y., and Mulani, P.M. (2009). Economic burden of psoriasis compared to the general population and stratified by disease severity. Curr. Med. Res. Opin. *25*, 2429–2438.

Yun, W.J., Lee, D.W., Chang, S.E., Yoon, G.S., Huh, J.R., Won, C.H., Lee, M.W., Kim, S.E., Kim, B.J., Moon, K.C., and Choi, J.H. (2010). Role of CD4CD25FOXP3 Regulatory T Cells in Psoriasis. Ann. Dermatol. *22*, 397–403.

STAR★METHODS

KEY RESOURCES TABLE

REAGENT or RESOURCE	SOURCE	IDENTIFIER
Antibodies		
anti-mouse CD45 clone 30-F11, Pacific Blue	BioLegend	Cat # 103125; RRID: AB_493536
anti-mouse CD3 clone 17A2, Alexa Fluor 700	Thermo Fisher Scientific	Cat# 56-0032-80; RRID: AB_529508
anti-mouse CD8a clone 53-6.7, PE-CF594	BD	Cat 562283; RRID: AB_11152075
anti-mouse CD4 clone RM4-5, Brilliant Violet 605	BioLegend	Cat# 100548; RRID: AB_2563054
anti-mouse Foxp3 clone FJK-16 s, PE	Thermo Fisher Scientific	Cat# 12-5773-80; AB_465935
anti-mouse CD11b clone M1/70, APC- Cy7	BD	Cat# 557657; AB_396772
anti-mouse Ki67 clone SolA15, PE- Cy7	Thermo Fisher Scientific	Cat# 25-5698-80; RRID: AB_11217689
anti-mouse TCR$\gamma\delta$ clone GL3, FITC	BioLegend	Cat# 118105; RRID: AB_313829
anti-mouse I-A/I-E clone M5/114.15.2, BB700	BD	Cat# 746197; RRID: AB_2743544
anti-mouse Ly-6G clone 1A8, BV650	BioLegend	Cat# 127641; RRID: AB_2565881
anti-mouse Ly-6G clone 1A8, Alexa Fluor 700	BioLegend	Cat# 127622; RRID: AB_10643269
anti-mouse Ly-6C clone AL-21, FITC	BD	Cat# 553104; RRID: AB_394628
anti-mouse Vγ5 clone 536, PE	BioLegend	Cat# 137504; RRID: AB_10550807
anti-mouse Vγ4 clone UC3-10A6, PerCP-eFluor 710	Thermo Fisher Scientific	Cat# 46-5828-80; RRID: AB_2573772
anti-mouse IL-17A clone TC11-18H10.1, PE-Cy7	BioLegend	Cat# 506922; RRID: AB_2125010
anti-mouse IL-22 clone IL22JOP, APC	Thermo Fisher Scientific	Cat# 17-7222-80; RRID: AB_10597584
anti-mouse CD11c clone N418, PE-Cy5.5	Thermo Fisher Scientific	Cat# 35-0114-82; RRID: AB_469709
anti-mouse IL-17F clone O79-289, PE-CF594	BD	Cat# 562418; RRID: AB_11154042
anti-mouse CD207 (Langerin) clone 4C7, APC	BioLegend	Cat# 144206; RRID: AB_2561998
anti-mouse CD14 clone Sa14-2, Brilliant Violet 510	BioLegend	Cat# 123323; RRID: AB_2564129
anti-mouse CD64 clone X54-5/7.1, Brilliant Violet 710	BioLegend	Cat# 139311; RRID: AB_2563846
anti-mouse CD24 clone M1/69, BUV496	BD	Cat# 564664; RRID: AB_2716853
anti-mouse CD103 clone 2E7, PE	BioLegend	Cat# 121406; RRID: AB_1133989
anti-mouse F4/80 clone BM8, PE-Cy5	BioLegend	Cat# 123111; RRID: AB_893494
anti-mouse B220 clone RA3-6B2, Brilliant Violet 785	BioLegend	Cat# 103245; RRID: AB_11218795
anti-mouse CD169 clone 3D6.112, Brilliant Violet 605	BioLegend	Cat# 142413; RRID: AB_2564030
anti-mouse CD69 clone H1.2F3, PE-Cy7	BD	Cat# 552879; RRID: AB_394508
anti-mouse CD62L clone MEL-14, FITC	BD	Cat# 553150; RRID: AB_394665
anti-mouse CD44 clone IM7, PE	BD	Cat# 55313; RRID: AB_394649
anti-mouse CD19 clone 6D5, Pacific Blue	BioLegend	Cat# 115523; RRID: AB_439718
anti-mouse TNF-α clone MP6-XT22, Brilliant Violet 711	BioLegend	Cat# 506349; RRID: AB_2629800
anti-mouse GM-CSF clone MP1-22E9, PE	Thermo Fisher Scientific	Cat# 12-7331-82; RRID: AB_466205
rat anti-human GM-CSF clone BVD2-21C11, APC	BD	Cat# 502309; RRID: AB_11148950
mouse anti-human Foxp3 clone 236A/E7	Thermo Fisher Scientific	Cat# 14-4777-80; RRID: AB_467555
rabbit anti-human CD3 clone SP7	Novus Biologicals	Cat# NB600-1441SS
Goat anti-rat Alexa Fluor 647	Thermo Fisher Scientific	Cat# A-21247; RRID: AB_141778
Goat anti-mouse Alexa Fluor 488	Thermo Fisher Scientific	Cat# A-11029; RRID: AB_138404
Goat anti-rabbit Alexa Fluor 555	Thermo Fisher Scientific	Cat# A-21428; RRID: AB_141784
LEAF Purified anti-mouse GM-CSF	BioLegend	Cat# 505407; AB_315383
anti-mouse GM-CSF clone MP1-31G6, Biotin	Thermo Fisher Scientific	Cat# 13-7332-85; RRID: AB_466949
anti-mouse CD45 clone 30-F11, Biotin	BioLegend	Cat# 103104; RRID: AB_312969
Chemicals, Peptides, and Recombinant Proteins		
Diphteria Toxin	Calbiochem	Cat# 322326
Aldara (5% Imiquimod)	3M Pharmaceuticals	N/A

(*Continued on next page*)

Continued		
REAGENT or RESOURCE	SOURCE	IDENTIFIER
PBS	Homemade	N/A
Ionomycin calcium salt from *Streptomyces conglobatus*	Sigma-Aldrich	CAS: 56092-82-1
Phorbol 12-myristate 13-acetate (PMA)	Sigma-Aldrich	CAS: 16561-29-8
Deoxyribonuclease (DNase) I from bovine pancreas	Sigma-Aldrich	CAS: 9003-98-9
Golgi Stop	BD	Cat# 554724
Golgi Plug	BD	Cat# 555029
Collagenase from *Clostridium histolyticum* (Collagenase IV)	Sigma-Aldrich	CAS: 9001-12-1
Avidin	Thermo Fisher Scientific	Cat# A2667
M-MLV reverse transcriptase	Invitrogen	Cat# 28025013
iTaq Universal SYBR Green Supermix	Bio-Rad	Cat# 1725124
SlowFade Gold antifade reagent with DAPI	Thermo Fisher Scientific	Cat# S36938
Cytofix/Cytoperm	BD	Cat#554714
eBioscience Foxp3/Transcription Factor Fixation/ Permeabilization Concentrate and Diluent	Thermo Fisher Scientific	Cat# 00-5521-00
Permeabilization Buffer	Homemade	N/A
Critical Commercial Assays		
RNeasy FFPE Kit	QIAGEN	Cat# 73509
Quick-RNA MiniPrep Kit	ZYMO RESEARCH	SKU 1054
Experimental Models: Organisms/Strains		
C57BL/6JRJ	The Janvier Labs	RRID:MGI:5752053
$Foxp3^{DTR/+}$: B6N.129(Cg)-$Foxp3^{tm3Ayr}$	provided by Markus Feurerer; Kim et al., 2007	N/A
$Csf2^{-/-}$: $Csf2^{tm1Jaw}$	provided by Glenn Dranoff; Dranoff et al., 1994	N/A
Oligonucleotides		
Primers for qPCR see Table S1	This paper	N/A
Software and Algorithms		
FlowJo v10.2	Tree Star	https://www.flowjo.com/
MATLAB R2016a	N/A	https://www.mathworks.com/
CYT	Amir et al., 2013	N/A
t-SNE	van der Maaten and Hinton, 2008	https://github.com/jkrijthe/Rtsne
FlowSOM	Van Gassen et al., 2015	https://github.com/SofieVG/FlowSOM
R studio	N/A	https://www.rstudio.com/
IMARIS	N/A	http://www.bitplane.com
GraphPad Prism 7	N/A	https://www.graphpad.com

CONTACT FOR REAGENT AND RESOURCE SHARING

Further information and requests for reagents should be directed to and will be fulfilled by Lead Contact Burkhard Becher (becher@immunology.uzh.ch).

EXPERIMENTAL MODEL AND SUBJECT DETAILS

Animal models

C57BL/6 mice (WT) were purchased from Janvier Laboratory. $Foxp3^{DTR/+}$ mice were generated by Kim et al. (2007) and kindly provided by Markus Feuerer (DKFZ Heidelberg, Germany). $Csf2^{-/-}$ mice were provided by Glenn Dranoff (Dranoff et al., 1994), backcrossed to C57BL/6 using speed congenics and crossed to $Foxp3^{DTR/+}$ mice. Male and female mice were used in all experiments (6-12 weeks old) and housed in specific pathogen free conditions. All experiments were approved by the Cantonal Veterinary Office Zurich.

Human studies

Analysis of retrospective patient samples from St.Gallen was approved by the local Research Ethics Committee (Ethikkommission Ostschweiz): BASEC- Project ID: 2016-01161 47 and EK800 entitled for the project entitled: "Retrospective histopathological characterization of lymph node metastases and correlation with response to immunotherapy in melanoma patients." Surplus tumor material was obtained after surgical removal of melanoma metastases from patients after written informed consent approved by the local IRB (EK647 and EK800).

Patient ID	Age	Sex	Treatment
HS18.18	36	f	no
HS18.27	29	f	no
K79c	31	f	no
K81b	57	f	no
K82d	27	m	no
K83a	45	f	no
H2015.8272	77	m	Ipilimumab
H2012.11567	64	m	Ipilimumab
B2011.58537	84	m	Ipilimumab
B2013.7833	84	m	Ipilimumab
HG2012.470	71	m	Ipilimumab
HG14.570	78	m	Ipilimumab

METHOD DETAILS

In vivo treatments

Mice were anesthetized with isoflurane and Aldara treatment was performed by applying daily 8 mg Aldara cream (5% Imiquimod; 3M Pharmaceuticals) on each mouse ear for the duration indicated in the text. DTx (Calbiochem, 500ng per mouse in PBS) was injected intraperitoneally (i.p.) on day 4 and 6 or 10 and 12 after starting the Aldara treatment. Anti-GM-CSF treatment was performed every second day by i.p. injection of 300 μg rat anti-mouse GM-CSF monoclonal Ab.

Tissue processing

Ears were cut into small pieces and digested in 5ml RPMI containing 1mg/ml Collagenase type IV and 100 μg/ml DNase I (both Sigma-Aldrich) while shaking at 37°C for 90 minutes. The tissue was further homogenized with a syringe and filtered through a 70 μm cell strainer. The cell strainer was washed with 20ml PBS followed by centrifugation (500 x g at 4°C for 10min).

Single cell suspensions from the LNs were obtained by mashing the LNs through 70 μm cell strainers. Single cells were then stained with fluorescence antibodies for Flow Cytometry.

Flow Cytometry

All utilized antibodies are summarized in the Key Resources Table. For surface staining, leukocytes isolated from the skin or the LNs were incubated with antibodies at 4°C for 20min. For intracellular cytokine staining, cells were re-stimulated in 1ml RPMI supplemented with Golgi-Stop or Golgi-Plug (1:1000, BD), PMA (50ng/ml, Applichem) and Ionomycin (500ng/ml, Invitrogen) for 4 hours at 37°C. After surface staining, cells were permeabilized and fixed in 200μl BD Cytofix/Cytoperm^{TM} according to the manufacturer's instructions. Then, cells were washed with Permeabilization buffer and stained intracellularly at 4°C for 20min in Permeabilization buffer. For intranuclear staining, cells were fixed and permeabilized using the eBioscience Foxp3/transcription factor fixation/permeabilization concentrate and diluent from ThermoFisher followed by incubation with antibodies at 4°C for 20min. Acquisition was performed with FACS LSRII Fortessa or FACSymphony (both BD). Flow cytometric analysis on live, single cells was performed using FlowJo (Tree Star) software.

For surface capture of GM-CSF expressing cells (Streeck et al., 2008), after re-stimulation with PMA and Ionomycin, cells were incubated with GM-CSF capture complexes consisting of biotin-labeled anti-GM-CSF and anti-CD45 antibodies linked by an avidin bridge. (Invitrogen). After cell surface staining $CD4^+$ and $CD4^+$ GM-CSF secreting T cells were sorted using FACS AriaIII 5L (BD).

Quantitative RT-PCR (qRT-PCR)

RNA was isolated from formalin-fixed, paraffin embedded tissue sections from healthy control skin or skin rashes of Ipilimumab-treated melanoma patients using the RNeasy FFPE Kit (QIAGEN) according to the manufactures instructions. RNA from snap-frozen human and murine skin or from sorted cells was isolated using the Quick-RNA MiniPrep Kit (Zymo Research). RNA was reverse transcribed to cDNA with M-MLV reverse transcriptase (Invitrogen). qRT-PCR was performed on a C1000 Touch Thermo Cycler (Bio-Rad) using SYBR Green (Bio-Rad) and primers described in Table S1. For DNA amplification a 3min incubation at 95°C was followed by 40 cycles with 10 s at 95°C and 45 s at 60°C.

Histology

For histo-pathological analysis, ear skin was fixed in HOPE, embedded in paraffin and 10 μm sections were cut using a microtome (Micro HM 325, Thermo Scientific). Subsequently, the sections were stained with hematoxylin and eosin (H&E) and were analyzed with a light microscope (Olympus BX41). Epidermal thickness was measured and cell infiltrates were counted on one representative image per sample. Mean of 3 measurements was calculated.

Immunofluorescence of human samples was performed on skin tissue from 3 biopsied healthy donors and 2 with Ipilimumab-associated dermatitis. Tissues were cryosectioned (12 μm thick) for immunofluorescence using a Hyrax C60 cryostat (Zeiss) and stored at −80°C. Skin sections were fixed in 2% PFA and acetone, washed in PBS, and blocked with PBS supplemented with 0.1% Triton X-100 and 4% normal goat serum. Subsequently, sections were incubated with the following primary antibodies (diluted in blocking solution) overnight at 4°C: rat anti-GM-CSF antibody (BD PharMingen, clone BVD2-21C11, 1:50), mouse anti-FoxP3 antibody (Invitrogen, clone 236A/E7, 1:20) and rabbit anti-CD3 (Novus, clone SP7, 1:100). Sections were then washed in PBS and incubated with AF647-labeled goat anti-rat, AF488-labeled goat anti-mouse and AF555-labeled goat anti-rabbit secondary antibodies (Life Technologies, 1:250-500) overnight at 4°C or at room temperature for 1 h. Sections were mounted with SlowFade Gold antifade reagent with DAPI (Invitrogen). Fluorescence photomicrographs were captured with a SP5 Leica confocal laser scanning microscope (SP5; Leica, Heerbrug, Switzerland) equipped with argon and helium lasers using the 40x or 60x objective (oil immersion, NA1.25 and NA 1.4 respectively). Images were processed and merged by Imaris imaging software (Bitplane, Zurich, Switzerland).

t-SNE visualization

FCS files of live, single cells were exported from FlowJo and transformed in CYT (MATLAB) (Amir et al., 2013) using the hyperbolic arcsine (arcsinh) function and percentile normalization in R. Pre-processed data was subsequently used as input for t-SNE visualization (van der Maaten and Hinton, 2008) and FlowSOM clustering (Van Gassen et al., 2015) following the workflow and script from Hartmann et al. (2016).

QUANTIFICATION AND STATISTICAL ANALYSIS

For disease curves, statistics were evaluated using 2-way ANOVA with Bonferroni's post-test. Differences between three or more experimental groups were analyzed using 1-way ANOVA. For comparison of two sets of data 2-tailed Student's t test was used. Statistical analysis was performed using GraphPad Prism (GraphPad Software). Statistical details of the data can be found in each figure legend. $p \leq 0.05$ was defined as significant.